Electron. Mater. Lett., Vol. 11, No. 1 (2015), pp. 155-163
DOI: 10.1007/s13391-014-4224-1

Depletion and Phase Transformation of a Submicron Ni(P) Film in the Early Stage of Soldering Reaction between Sn-Ag-Cu and Au/Pd(P)/Ni(P)/Cu

Cheng-En Ho,* Wan-Zhen Hsieh, and Tsung-Hsun Yang

Department of Chemical Engineering & Materials Science, Yuan Ze University, Chungli City, Taiwan, R.O.C.

(received date: 4 August 2014 / accepted date: 10 September 2014 / published date: 10 January 2015)

The early stage of soldering reaction between Sn-3Ag-0.5Cu solder and ultrathin-Ni(P)-type Au/Pd(P)/Ni(P)/Cu pad was investigated by field-emission scanning electron microscopy (FE-SEM) in conjunction with field-emission electron probe microanalysis (FE-EPMA) and high-resolution transmission electron microscopy (HRTEM). FE-SEM, FE-EPMA, and HRTEM investigations showed that Ni_2SnP and Ni_3P were the predominant P-containing intermetallic compounds (IMCs) in the soldering reaction and that their growth behaviors strongly depended on the depletion of Ni(P). The growth of Ni_3P dominated over that of Ni_2SnP in the early stage of soldering, whereas the Ni_3P gradually transformed into Ni_2SnP after Ni(P) depletion. This Ni(P)-depletion-induced Ni_2SnP growth behavior is different from the reaction mechanisms reported in the literature. Detailed analyses of the microstructural evolution of the IMC during Ni(P) depletion were conducted, and a two-stage reaction mechanism was proposed to rationalize the unique IMC growth behavior.

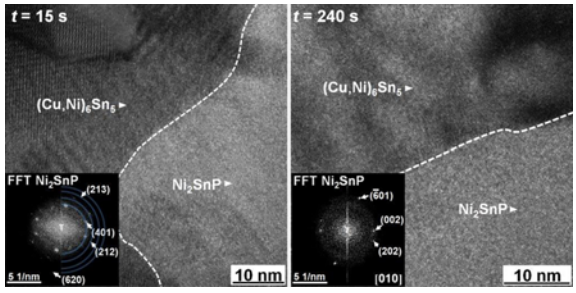

Keywords: Au/Pd(P)/Ni(P)/Cu, submicron Ni(P), Sn-Ag-Cu, Ni_2SnP

1. INTRODUCTION

Sequential deposition of submicron-scale Ni(P), Pd(P), and Au films over Cu metallization pads has recently attracted a great deal of attention in the electronic industry because this ultrathin surface finish [Au/Pd(P)/Ni(P)] meets the requirements of fine-pitch packaging and signal stability for high-frequency operation, such as radio frequency (RF) filters and duplexers.[1-3] Previous studies have shown that submicron-scale Au, Pd(P), and Ni(P) films can be depleted in a sequential order within a few seconds of soldering reaction.[4-8] The depletion of Ni(P) exposes the underlying Cu pad to molten solder, and an aggressive reaction between the solder and the Cu pad occurs in the absence of the Ni(P) diffusion barrier. The series of soldering reactions might produce a multilayer of intermetallic compounds (IMCs), including $(Cu,Ni)_6Sn_5$ (high Ni containing), Ni_2SnP, Ni_3P, Cu_6Sn_5 (low Ni containing), and Cu_3Sn,[5-8] which is distinctly different from the microstructure obtained in a Sn-Ag-Cu/Au/Pd(P)/Ni(P)/Cu reaction system with micro-scale Ni(P) deposits.[6-12] Additionally, numerous micro-/nano-voids might also be created in these IMCs, especially in Ni_2SnP, Ni_3P, and Cu_6Sn_5 (low Ni containing). Because IMCs are generally brittle in nature, the formation of a multilayer IMC structure accompanied by voids is highly detrimental to the solderability and degrades the mechanical reliability of solder joints.[5-8,10,13] The abovementioned preliminary studies have confirmed that the interfacial reaction between solder (Sn-Ag-Cu) and Au/Pd(P)/Ni(P)/Cu and the resulting mechanical properties are strongly dependent on the thickness of the Ni(P) layer.[5-8] These dependencies are closely related to the extent of Ni(P) depletion. However, the reaction mechanism governing this Ni(P) depletion and the depletion-induced phase transformation in the solder/submicron-Ni(P)/Cu reaction system are still not well established. In this study, the early stage of soldering reaction between Sn-Ag-Cu and Au/Pd(P)/Ni(P)/Cu pad (ultrathin-Ni(P)-type) was investigated. The evolution of the interfacial microstructure before and after Ni(P) depletion was characterized by field-emission scanning electron microscopy (FE-SEM) in conjunction with electron probe

*Corresponding author: ceho1975@hotmail.com

microanalysis (FE-EPMA) and high-resolution transmission electron microscopy (HRTEM). Furthermore, the correlation between Ni(P) depletion and the resulting IMC transformation was discussed.

2. EXPERIMENTAL PROCEDURE

The early stage of soldering reaction between 96.5 wt. % Sn-3 wt. % Ag-0.5 wt. % Cu alloy (termed Sn-3Ag-0.5Cu) and Au/Pd(P)/Ni(P)/Cu multilayer was investigated. The Au/Pd(P)/Ni(P) trilayer (thickness: 0.1 μm/0.2 μm/0.9 μm) was deposited over Cu pads with a thickness of 20 μm and an opening diameter of 235 μm. The thicknesses of the layers were determined using a calibrated x-ray fluorescence spectrometer and subsequently verified via focused ion beam (FIB) cross-sectional analysis, as shown in Fig. 1. A small amount of P, (2% to 5%)/(6% to 8%), was codeposited with the Pd/Ni platings due to the use of an alkaline solution of hypophosphite in the electroless plating process.[9] Consequently, the average compositions of Pd(P) and Ni(P) were approximately 96.5 wt. % Pd-3.5 wt. % P (or $Pd_{0.89}P_{0.11}$, mole fraction) and 93 wt. % Ni-7 wt. % P (or $Ni_{0.88}P_{0.12}$, mole fraction), respectively. Before soldering, Sn-3Ag-0.5Cu solder balls (diameter: 300 μm) were dipped into a rosin mildly activated flux and were then planted onto the Au/Pd(P)/Ni(P)/Cu pads. During soldering, the reaction temperature was fixed at 240(±3) °C and the reaction time (t) ranged from 15 s to 240 s (~3 reflows). After soldering, the solder joints were immediately quenched in water and were then subjected to a metallographically grinding-polishing process to reveal the interior microstructures.

The interfacial microstructure between Sn-3Ag-0.5Cu and Au/Pd(P)/Ni(P)/Cu was examined using FE-SEM (type: JEOL 6701F) and HRTEM (type: JEOL JEM-2100F) operated at 200 keV. The composition of the reaction product species was determined using FE-EPMA (type: JEOL JXA-8500F) operated at 12 keV. Additionally, each phase present in the reaction zone was identified by TEM selected-area diffraction patterns (SADPs) and nano-beam diffraction patterns (NBDPs), combined with energy dispersive x-ray spectroscopy (EDS). The beam sizes utilized in the SAD and NBD analysis were ~180 nm and less than 5 nm, respectively. The specimens used for the HRTEM examination were prepared using FIB.

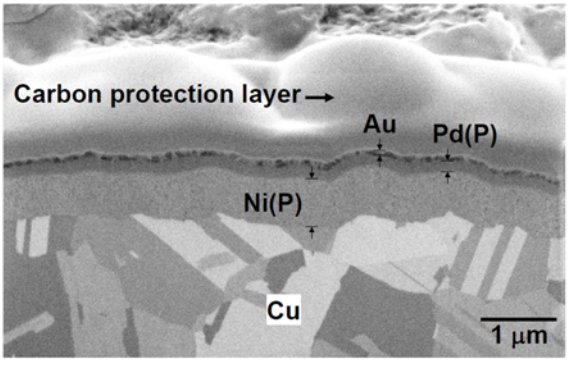

Fig. 1. FIB-processed cross section of the Au/Pd(P)/Ni(P)/Cu metallization pad prior to soldering reaction.

3. RESULTS

Figure 2(a)-(c) shows the interface between Sn-3Ag-0.5Cu and Au/Pd(P)/Ni(P)/Cu after reacting at 240°C for t = 15 - 45 s, displaying the evolution of the interfacial microstructure in the early stage of soldering reaction. Several facet-like grains scattered at the interface can be noted at t = 15 s. These grains were identified by FE-EPMA to be Cu_6Sn_5 incorporated with a large amount of Ni (approximately 16 - 22 at. %) and a small amount of Pd (less than 1 at. %), termed $(Cu,Ni)_6Sn_5$ hereafter. The grain size of $(Cu,Ni)_6Sn_5$ did not markedly alter (Fig. 2(a)-(c)), but the number of grains readily increased during this reaction period (t = 15 - 45 s), thereby creating a layered $(Cu,Ni)_6Sn_5$ structure at the interface after 45 s (Fig. 2(c)). Between $(Cu,Ni)_6Sn_5$ and Cu, no meaningful Au and Pd signals were detectable by FE-EPMA analysis, and only a continuous (Ni, P)-rich zone existed after 15 s. Identification of the (Ni, P)-rich zone via FE-EPMA showed that the zone predominantly consisted of three phases, Ni-Sn-P, Ni_3P, and Ni(P). These observations indicate that the surface layers of Au/Pd(P) had been quickly eliminated from the interface in few seconds of soldering, leaving the underlying Ni(P) in the reaction zone.

Figure 2(d) shows the interfacial microstructure observed after prolonging t to 60 s, demonstrating that a portion of the Cu began to react with the solder. The image provides evidence that a 0.9-μm Ni(P) film cannot function as an efficient diffusion barrier against molten solder at reaction time exceeding 60 s and that the solder could penetrate to the underlying Cu substrate after the breakdown of the Ni(P) barrier. The solder/Cu reaction yielded a second Cu_6Sn_5 layer (possibly with Cu_3Sn) beneath the (Ni, P)-rich zone, as shown in Fig. 2(d)-(f). Because the second Cu_6Sn_5 layer dissolved with a much lower Ni content (approximately 6 at. %) than did the $(Cu,Ni)_6Sn_5$ phase, this low-Ni-containing phase is therefore referred to as Cu_6Sn_5 to distinguish it from the high-Ni-containing one [i.e., $(Cu,Ni)_6Sn_5$] resulting from the solder/Ni(P) reaction (Fig. 2(a)-(c)). Between $(Cu,Ni)_6Sn_5$ and Cu_6Sn_5, the original (Ni, P)-rich zone was entirely converted to a Ni-Sn-P layer incorporated with a small amount of Cu (approximately 4 at. %) (Fig. 2(d)-(f)). Our preliminary analysis of the ring diffraction pattern obtained by TEM showed that the Ni-Sn-P(Cu) layer was a mixture layer composed of Ni_2SnP and $(Cu,Ni)_6Sn_5$.[6] However, the phase formation and transformation of $Ni_2SnP + Ni_3P + Ni(P)$ into Ni_2SnP in this

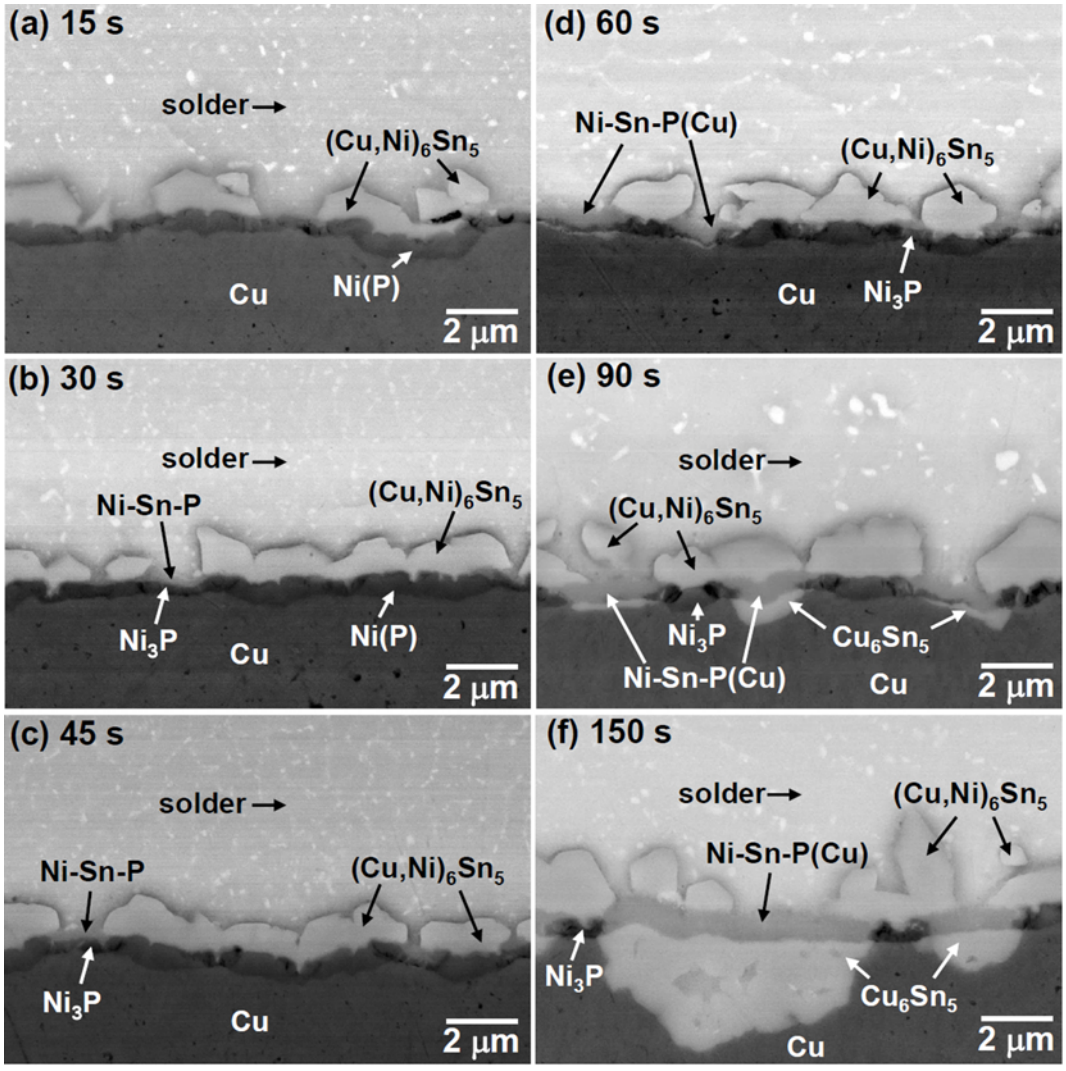

Fig. 2. Backscattered electron micrographs showing the reaction zone between Sn-3Ag-0.5Cu and Au/Pd(P)/Ni(P)/Cu after soldering at 240°C for t = 15 s (a), 30 s (b), 45 s (c), 60 s (d), 90 s (e), and 150 s (f).

submicron region were still not well established, and thus, further TEM characterization was conducted.

Figure 3(a) shows a bright-field scanning transmission electron microscopy (BF-STEM) image, displaying a magnified view of the solder/Cu interface shown in Fig. 2(a). Non-uniform growth of $(Cu,Ni)_6Sn_5$ is clearly observed in this STEM image. The results of electron diffraction analysis, shown in SADP1 (the inset of Fig. 3), demonstrate that $(Cu,Ni)_6Sn_5$ is based on the hexagonal close-packed (HCP) η-Cu_6Sn_5 structure rather than the monoclinic η'-Cu_6Sn_5 structure. The results of diffraction analysis agree with those reported in previous studies,[4,12,14] which is consistent with the viewpoint that the incorporation of an appropriate amount of Ni into Cu_6Sn_5 allows for the stabilization of the high-temperature phase (η) at low temperature, i.e., below 186°C.[15] Figure 3(b) shows a magnified image of the $(Cu,Ni)_6Sn_5$/Cu interface in Fig. 3(a), providing a detailed view of the (Ni, P)-rich zone. Three adjacent phases between $(Cu,Ni)_6Sn_5$ and Cu can be resolved in the TEM image. From top to bottom, the average composition of each phase was determined by TEM-EDS to be 52.4 at. % Ni-31.8 at. % Sn-15.8 at. % P, 76.6 at. % Ni-23.4 at. % P, and 89.5 at. % Ni-10.5 at. % P. The first phase (i.e., 52.4 at. % Ni-31.8 at. % Sn-15.8 at. % P) with an average thickness of approximately 80 nm is likely Ni_2SnP, as reported in the literature.[6,10,12,16-20] Further nano-beam diffraction analysis verified this assumption, i.e., that the Ni-Sn-P phase is isomorphous with orthorhombic Ni_2SnP (NBDP, Fig. 3). TEM investigation revealed that Ni_2SnP was the predominant compound layer adjacent to the solder in the region not covered with the $(Cu,Ni)_6Sn_5$ layer. Direct contact of Ni_2SnP with solder has also been observed in a previous study.[10] It was reported that the growth of Ni_2SnP dominated over that of $(Cu,Ni)_6Sn_5$ in the early stage of

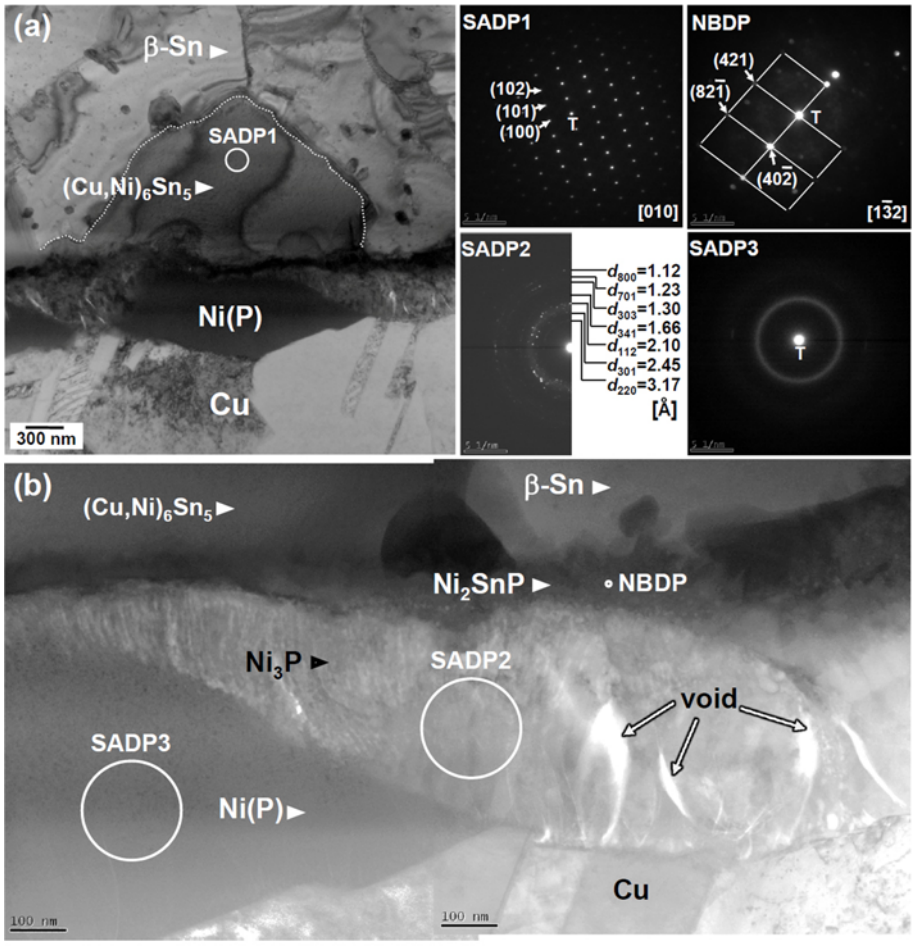

Fig. 3. (a) BF-STEM micrograph of the reaction zone shown in Fig. 2(a), together with a selected-area diffraction pattern taken from $(Cu,Ni)_6Sn_5$ (SADP1). (b) Magnified image of the interface between $(Cu,Ni)_6Sn_5$ and Cu in (a), together with electron diffraction patterns taken from Ni_2SnP (NBDP), Ni_3P (SADP2), and Ni(P) (SADP3).

soldering reaction, especially when a thick Pd(P) film was utilized.

The composition of the second phase (i.e., 76.6 at. % Ni-23.4 at. % P) corresponds to the stoichiometry of Ni_3P. Numerous columnar voids formed in the Ni_3P layer (Fig. 3(b)), in good agreement with the findings of Chen *et al.*.[21,22] The presence of these voids between the $(Cu,Ni)_6Sn_5$ IMC and the Ni(P) film is likely the root cause of the reduction in shearing resistance of solder joints under a high strain rate test.[23] The selected-area diffraction pattern taken from this phase exhibits discontinuous Debye rings, as shown in SADP2 (Fig. 3), indicating that the phase possessed a polycrystalline structure. The third phase (i.e., 89.5 at. % Ni-10.5 at. % P) formed between Ni_3P and Cu was the residual Ni(P) film, whose SADP shows a broad, dim ring (SADP3), indicating that the Ni(P) film possessed an amorphous structure. The amorphous Ni(P) differs from that examined in the literature,[4] in which the Ni(<5 wt. % P) film possessed a polycrystalline structure. This microstructural difference is closely related to the P content in the electroless Ni(P) deposit; namely, a high P-containing Ni(P) alloy (>9.5 at. % or 5.3 wt. %) exhibits an amorphous character, whereas a polycrystalline structure is obtained when the P content is less than 9.5 at. %.[24]

Figure 4(a) shows a BF-STEM image of the interfacial microstructure between Sn-3Ag-0.5Cu and Au/Pd(P)/Ni(P)/Cu after a long-term soldering reaction (three typical reflow cycles, $t \approx 240$ s). The Au/Pd(P)/Ni(P) trilayer was completely depleted and produced a multilayer of $(Cu,Ni)_6Sn_5$/Ni-Sn-P(Cu)/Cu_6Sn_5 at the solder/Cu interface, which is analogous to the microstructure obtained in Fig. 2(f). Selected-area diffraction analyses of $(Cu,Ni)_6Sn_5$ (SADP1) and Cu_6Sn_5 (SADP2) reveal that both of the phases matched well with the HCP η-Cu_6Sn_5 structure, independent of the Ni content. This TEM result provides a clarification in the dispute regarding which crystal structure is adopted by the Cu_6Sn_5 phase (η or η') because both of the aforementioned Cu_6Sn_5 dissolved with different amounts of Ni and coexisted at the

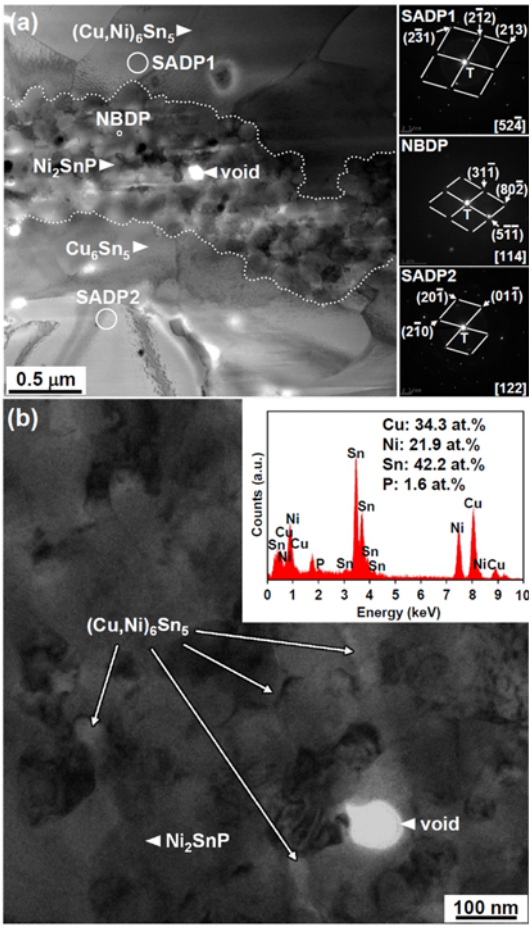

Fig. 4. (a) BF-STEM micrograph of the $(Cu,Ni)_6Sn_5/Ni_2SnP$ + $(Cu,Ni)_6Sn_5/Cu_6Sn_5$ trilayer, together with electron diffraction patterns taken from $(Cu,Ni)_6Sn_5$ (SADP1), Ni_2SnP (NBDP), and Cu_6Sn_5 (SADP2). (b) Magnified image of the Ni_2SnP + $(Cu,Ni)_6Sn_5$ layer shown in (a), along with an EDS spectrum obtained from $(Cu,Ni)_6Sn_5$ that grew among the Ni_2SnP nanocrystals.

interface.[6] The BF-STEM image also shows that the intermediate layer [i.e., Ni-Sn-P(Cu)] consisted of many nanocrystals with an average grain size of approximately 110 nm and had an overall thickness of approximately 0.6 μm. The NBDP gathered from one of the nanocrystals (as marked by a circle indicated with NBDP) indicates that the nanocrystals belong to the Ni_2SnP phase, validating the analysis of ring diffraction pattern performed in a previous study.[6] Several nanovoids were observed among these Ni_2SnP grains. This observation demonstrates that the polycrystalline Ni_3P with columnar voids formed in the early stage of soldering reaction (Fig. 3) was completely converted to nanocrystalline Ni_2SnP accompanied by nanovoids by prolonging *t*. Further TEM/EDS analysis (Fig. 4(b)) shows that the spacings among the Ni_2SnP grains were actually filled with $(Cu,Ni)_6Sn_5$ such that a certain amount of Cu (~4 at. %) was detectable in this intermediate layer by EPMA analysis. This finding confirms that the Ni-Sn-P(Cu) layer was indeed a mixed layer consisting of two different IMCs, Ni_2SnP and $(Cu,Ni)_6Sn_5$.[6] The incorporation of $(Cu,Ni)_6Sn_5$ among the Ni_2SnP grains suggests that interdiffusion between Cu and Sn occurred after the breakdown of the Ni(P) diffusion barrier. Because the Ni_2SnP layer possessed a nanocrystalline structure, instead of a dense layer, the grain boundaries might provide shortcuts to facilitate the interdiffusion between Cu and Sn.[6]

A comparison of the Ni_2SnP phase shown in Fig. 3 (t = 15 s) and that shown in Fig. 4 (t = 240 s) reveals significant differences not only in the growth thickness (0.08 μm and 0.6 μm, respectively) but also in the microstructure. Figure 5(a)-(b) shows HRTEM images, providing a detailed view of the Ni_2SnP microstructure formed at t = 15 s and 240 s, respectively. The difference in crystallinity can be clearly visualized with the aids of HRTEM. The Ni_2SnP formed at t = 240 s showed a highly ordered atomic arrangement (Fig. 5(b)), whereas the same phase formed in the early stage of soldering reaction (t = 15 s) displayed relative disorder among atoms (Fig. 5(a)), indicating that the crystallinity of Ni_2SnP may be enhanced by prolonging *t*. To obtain more quantitative evidence, electron diffraction analysis was then performed to evaluate the crystallinity of the Ni_2SnP phase at these two different reaction stages. The insets (Fig. 5(a') and 5(b')) show electron diffraction patterns captured for Ni_2SnP at t = 15 s and 240 s, which were obtained using the lattice images simulated by fast Fourier transform (FFT) through the Gatan DigitalMicrograph software. The FFT image, as shown in Fig. 5(a'), consists of numerous diffraction spots, most of which match well with the reciprocal lattice of Ni_2SnP. The arrangement of several diffraction spots on concentric rings in the FFT spectra (Fig. 5(a')) indicates the existence of several grains with different orientations. In contrast, indexation of the FFT image captured at t = 240 s (Fig. 5(b')) shows a single crystalline structure with the indexed zone of [010]. The FFT analyses confirm the differences in the crystallinity of Ni_2SnP observed at different soldering reaction times, with high crystallinity achieved after a long-term soldering reaction.

The irregular depletion of the Ni(P) film, accompanied by the non-uniform growth of Ni_3P and Ni_2SnP, can also be noted in Fig. 2-3. This microstructural appearance is strongly correlated with the growth morphology of $(Cu,Ni)_6Sn_5$. Specifically, the Ni(P) film was seriously exhausted in the region not covered with $(Cu,Ni)_6Sn_5$, where the Ni_2SnP substituted for $(Cu,Ni)_6Sn_5$ adjacent to the solder and a thick Ni_3P formed beneath this Ni_2SnP, as shown in Fig. 3(b). In contrast, only a moderate depletion of Ni(P) along with relatively thin Ni_3P and Ni_2SnP layers occurred at the interface covered with $(Cu,Ni)_6Sn_5$. This finding implies that only a few Ni atoms diffused out of the Ni(P) film covered with $(Cu,Ni)_6Sn_5$, which in turn supports the views that the

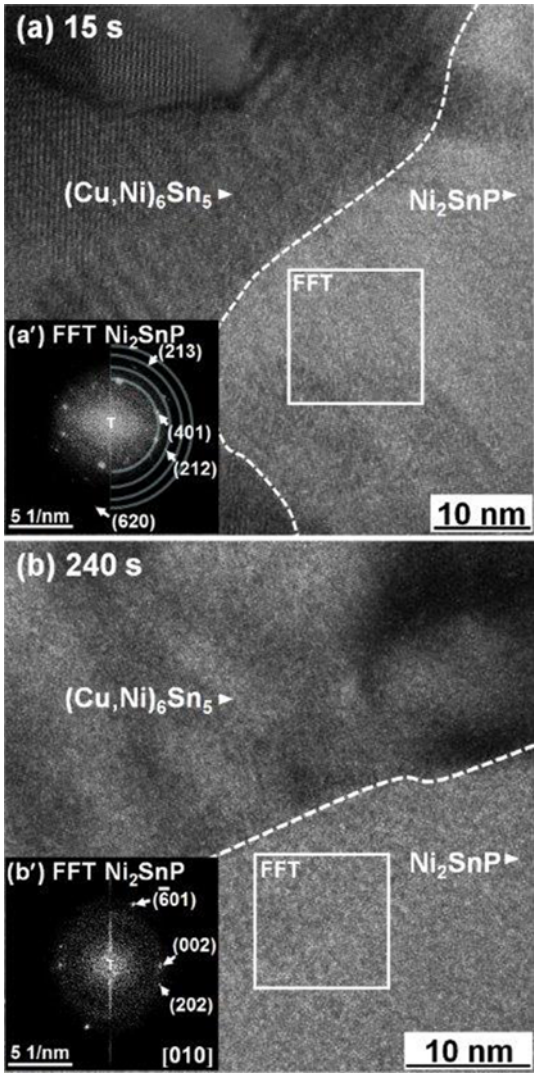

Fig. 5. (a) HRTEM image of the $(Cu,Ni)_6Sn_5/Ni_2SnP$ interface for t = 15 s, together with a FFT pattern (a') obtained from the area marked with a square; (b) same as (a) but for $t \approx 240$ s (3 reflows).

growth morphology of $(Cu,Ni)_6Sn_5$ dominated the Ni(P) depletion behavior and that a dense $(Cu,Ni)_6Sn_5$ layer can behave as an effective barrier against Ni depletion/diffusion.[12,25] It is emphasized that irregular Ni(P) depletion and non-uniform IMC growth were not observed in the case of a *thick* Ni(P) film,[26] even though the Ni(P) films (3.9 - 9.9 μm) had been entirely depleted after a long-term reaction. In Chen's study,[26] a Cu-free solder (Sn-3.5Ag) was subjected to solid-state reaction with Ni(P) metallization at 160°C - 200°C, and the predominant IMC species formed at the solder/Ni_2SnP interface was a uniform, dense Ni_3Sn_4 layer, instead of a discontinuous $(Cu,Ni)_6Sn_5$ (Fig. 2 - 3). The differences in the IMC species and growth morphology provide a possible explanation concerning why the Ni(P) depletion observed in this study behaved in a different manner from that in the thick-Ni(P) case.[26]

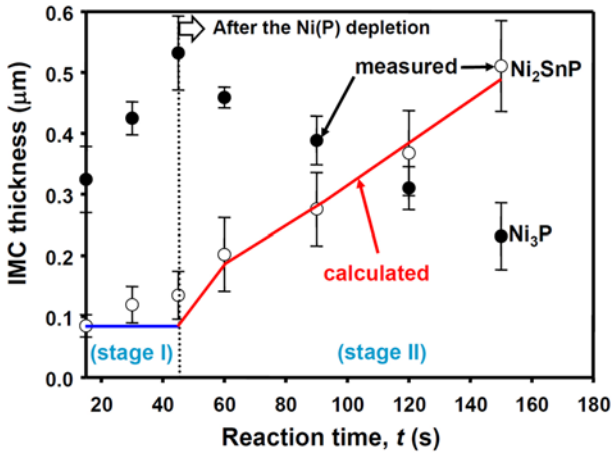

Fig. 6. Growth thicknesses of Ni_2SnP and Ni_3P as functions of t. The dark and white circles depict the measured thicknesses of Ni_3P and Ni_2SnP, respectively. The solid lines represent the calculated thickness of Ni_2SnP.

The growth thicknesses of Ni_3P (δ_{Ni_3P}) and Ni_2SnP (δ_{Ni_2SnP}) as functions of t are plotted in Fig. 6, which provides a quantitative description of the IMC growth behavior before and after Ni(P) depletion. The thickness of the IMC layer was defined as the total area of the phase divided by the linear length of the interface. The measurements were performed using calibrated image analysis software combined with an optical microscopy system, and the global mean values with error bars were plotted in the figure. The growth of Ni_2SnP (depicted by white circles) and Ni_3P (depicted by dark circles) could be approximately divided into two stages according to t: (stage I)—before Ni(P) depletion (t = 15 - 45 s); (stage II)—after Ni(P) depletion (t = 45 - 150 s), as illustrated in Fig. 6. In stage I, δ_{Ni_3P} increased from 0.32 μm to 0.53 μm, whereas δ_{Ni_2SnP} remained at a constant value of approximately 0.1 μm, indicating that the growth of Ni_3P was dominant in the first stage of the soldering reaction, during which the Ni(P) film still persisted. The entire Ni(P) film was approximately depleted at t = 45 s (Fig. 2(c)). Afterwards, δ_{Ni_3P} stopped increasing and began to decrease from 0.53 μm (45 s) to 0.23 μm (150 s), whereas δ_{Ni_2SnP} dramatically increased from 0.14 μm to 0.51 μm, as shown in Fig. 6. The transition in the IMC growth behavior is discussed in the next section.

4. DISCUSSIONS

The research results show that the growth of the P-containing IMCs (Ni_3P and Ni_2SnP) was strongly dependent on the Ni(P) depletion. It is clear that there are two stages in the growth of the Ni_3P and Ni_2SnP phases, as depicted in Fig. 6. The growth of Ni_3P dominated over that of Ni_2SnP in the early stage of soldering (t = 15 - 45 s), whereas the Ni_3P phase gradually transformed into the Ni_2SnP phase after

Ni(P) depletion (t = 45 - 150 s). The decrease in the content of the Ni_3P phase and the increase in that of the Ni_2SnP phase indicate that the growth of the former phase (Ni_3P) was unstable, whereas that of the latter phase (Ni_2SnP) was stable after the depletion of the Ni(P) film. To interpret this phenomenon before and after Ni(P) depletion, an ideal mass conservation reaction was used to investigate the IMC growth behavior in the two stages. We assumed that all of the P from either Pd(P) or Ni_3P was eventually converted to Ni_2SnP at the interface, that is, no P loss into the solder occurred during the soldering reaction. Additionally, only the solder/Pd(P) (or Sn/$Pd_{0.89}P_{0.11}$) reaction was considered in the first stage, whereas the solder/Ni_3P reaction is introduced in the second stage. Based on these assumptions, the reaction equations relevant to Ni_2SnP formation are as follows:

$$\text{Stage I: } Pd_{0.89}P_{0.11} + 0.11Sn + 0.22Ni \rightarrow 0.11Ni_2SnP + 0.89Pd \quad (1)$$

$$\text{Stage II: } Ni_3P + Sn \rightarrow Ni_2SnP + Ni \quad (2)$$

According to Eq. (1), 1 mole of $Pd_{0.89}P_{0.11}$ can produce 0.11 mole of Ni_2SnP (stage I). In stage II, for 1 mole of Ni_3P, 1 mole of Ni_2SnP is yielded (Eq. (2)). The remaining free Pd and Ni in Eq. (1)-(2) would either be reacted into IMC(s), e.g., $(Pd,Ni)Sn_4$ and $(Cu,Ni)_6Sn_5$, or dissolve into the solder. Based on the correlations established in Eq. (1)-(2), δ_{Ni_2SnP} can be estimated according to the following equation:

$$\delta_{Ni_2SnP} = \Sigma\left(\frac{\Omega_{Ni_2SnP}}{\Omega_i} \times \Delta\delta_i \times n_i\right) \quad (3)$$

where Ω_{Ni_2SnP} and Ω_i are the molar volumes of Ni_2SnP and phase i, respectively; n_i is the ratio of the number of moles of Ni_2SnP to that of phase i in Eq. (1) and (2); and $\Delta\delta_i$ is the reduced thickness of phase i, where i = Pd(P) and Ni_3P in this study.

Because only a limited amount of P (3.5 wt. % or 11 at. %) was incorporated into the Pd layer, the molar volume of Pd(P) ($\Omega_{Pd(P)}$) was approximately equal to that of pure Pd, i.e., 8.9 cm^3/mol.[27] The Ω_{Ni_2SnP} and Ω_{Ni_3P} values can be acquired by dividing the molecular weight of the phase by the density, which are approximately 35.3 cm^3/mol and 26.5 cm^3/mol, respectively. $\Delta\delta_{Pd(P)}$ is 0.2 μm after 15 s because of the complete exhaustion of the Pd(P) film in the early stage of soldering reaction, as evidenced in Fig. 2(a) and 3. The $\Delta\delta_{Ni_3P}$ value is dependent on t and would gradually enlarge at t = 45 - 150 s (i.e., stage II, Fig. 6) as a result of the reaction shown in Eq. (2). According to Eq. (1) - (2), $n_{Pd(P)}$ and n_{Ni_3P} are 0.11 and 1, respectively. Insertion of all of the required parameters into Eq. (3) yields

$$\delta_{Ni_2SnP} \approx 0.09 + 1.33\Delta\delta_{Ni_3P} \ [\mu m] \quad (4)$$

The first term on the right-hand side of Eq. (4) (0.09 μm) results from the Sn/Pd(P) reaction, as indicated in Eq. (1), approximating the measured values (0.085 - 0.13 μm for t = 15 - 45 s) obtained for stage I (depicted by a blue solid line in Fig. 6). A gradual increase in the deviation between the calculated result (0.09 μm) and the measured value can also be noted in Fig. 6. This gradually increased deviation might result from the solder/Ni_3P reaction (Eq. (2)), which is not considered in the stage I reaction. The second term on the right-hand side of Eq. (4), i.e., 1.33 $\Delta\delta_{Ni_3P}$, results from the Sn/Ni_3P reaction (Eq. (2)), where $\Delta\delta_{Ni_3P}$ (i.e., the reduced thickness of Ni_3P) increases as a function of t in stage II (Fig. 6). By inserting the measured $\Delta\delta_{Ni_3P}$ data into Eq. (4), the value of δ_{Ni_2SnP} was calculated as a function of t and plotted in Fig. 6 (depicted by a red solid line). The calculated values match well with the measured data (white circles). This good agreement verifies the assumption that all of the P from either Pd(P) or Ni_3P was converted to Ni_2SnP at the interface without P loss to the solder during the soldering reaction. This observation also provides evidence that the transformation of Ni_3P into Ni_2SnP (i.e., Eq. (2)) was initiated at $t \approx 45$ s (Fig. 6), where the Ni(P) film was completely depleted, as shown in Fig. 2(c).

The growth and reduction of the IMC(s), as shown in Fig. 2-6, indicates that the Ni(P) depletion might induce the transformation of Ni_3P into Ni_2SnP. According to the literature, two classical reaction mechanisms regarding Ni_2SnP formation have been reported.[10,14,17-19] The reaction mechanism presented in Ref.[17-19] refers to the P content in the Ni(P) film. Duh *et al.*[17-19] observed that Ni_2SnP formation was derived from the inward diffusion of Sn to Ni_2P, which was the exclusive reaction product species that was yielded when Sn-3Ag-0.5Cu solder reacted with a high-Ni-containing Ni(P) substrate (13 wt. % P). Thus, the growth behavior of Ni_2SnP in such a case is dominated by both the formation of a specific phase (Ni_2P) and atomic (Sn) diffusion. Because the P content of the Ni(P) film examined in the present study was low (6 - 8 wt. %), the Ni_2P phase had difficulties in nucleating at the interface. In other words, the Ni_2SnP growth behavior in either stage I or II (Fig. 6) did not correspond to the mechanism proposed by Duh *et al.*.[17-19] The alternative reaction mechanism proposed by Ho *et al.*[10] refers to the effect of the Pd(P) film. Ho *et al*.[10] argued that P atoms would separate from the Pd(P) film and subsequently crystallize with Sn and Ni as Ni_2SnP at the interface in an early stage of soldering reaction. This Ni_2SnP growth behavior is based on the mass conservation of P, as mathematically described in Eq. (3), and was experimentally verified in Ref..[14] The thickness of the Pd(P) film deposited on the Ni(P) film was 0.2 μm in this study, which might yield an approximately 0.09-μm-thick Ni_2SnP after the soldering reaction, according to Eq. (3). The growth behavior of Ni_2SnP that occurred in stage I (Fig. 6) agrees well with the calculated results based on the reaction mechanism proposed by Ho *et al.*.[10,14] However, the growth of the

Ni_2SnP phase in stage II resulted from the transformation of Ni_3P into Ni_2SnP, as depicted in Eq. (2), which is induced by the depletion of the Ni(P) film, as shown in Fig. 2-6. This Ni(P)-depletion-induced Ni_2SnP growth behavior is different from the reaction mechanisms reported in previous studies[10,14,17-19] and has rarely been observed in the case of a thick Ni(P) film submitted to a typical soldering process. The differences in the crystallinity of Ni_2SnP (Fig. 5) provide evidence of the different reaction mechanisms that occur in stage I and II.

Numerous micro-sized voids with a columnar morphology in the Ni_3P layer are observed in the BF-STEM image shown in Fig. 3(b), which might seriously deteriorate the mechanical reliability of the joint interface.[21,22] The formation of voids can be ascribed to the fast out-diffusion of Ni through Ni_3P toward the solder, accumulating vacancies for the nucleation of voids.[21,22] Recently, Chen *et al.*[21,22] proposed that the incorporation of a third element (e.g., Co or W) into electroless Ni(P) alloy can be an effective way to inhibit voiding in Ni_3P. It was observed that the doped Co retarded the growth rates of all of the IMCs at the interface, thereby inhibiting void formation as well as Ni(P) depletion.[22] The doped Co would dissolve into the Ni sublattice of Ni_3P, forming a ternary $(Ni,Co)_3P$ layer. Although the $(Ni,Co)_3P$ has a crystal structure based on that of Ni_3P, it did not display a columnar Ni_3P structure (Fig. 3(b)), and only nano-sized voids were created inside the $(Ni,Co)_3P$ layer due to the overall slow interfacial reaction.[22] Alternatively, the doped W yielded an amorphous $(Ni,W)_3P$ structure.[21] Because the $(Ni,W)_3P$ phase is free of fast diffusion channels such as grain boundaries, it is even more difficult for Ni atoms to diffuse out through this layer; thereby, no voids were observed by SEM.[21] Accordingly, the long-term reliability of Ni(P) can be significantly enhanced by incorporating W (or Co) into the Ni(P) film. The results shown in Fig. 4 further reveal that the micro-sized voids in Ni_3P may have been completely eliminated from the interface by converting Ni_3P to Ni_2SnP. This observation suggests that the net atomic flux was in the direction from the solder region toward the Cu substrate after Ni(P) depletion, which is opposite to the Ni diffusion in the solder/Ni(P) reaction. This also implies that the in-diffusion of Sn towards the Cu substrate is greater than the out-diffusion of Ni towards the solder when the reaction of Eq. (2) occurs. The microstructure transition from Ni_3P to Ni_2SnP provides an alternative approach to reducing void formation at the joint interface.

5. CONCLUSIONS

The early stage of soldering reaction between Sn-3Ag-0.5Cu solder and Au/Pd(P)/Ni(P)/Cu pad with film thicknesses of 0.1 μm/0.2 μm/0.9 μm/20 μm was investigated by FE-SEM, FE-EPMA, and HRTEM in this study. Before the depletion of the Ni(P) film, the predominant IMCs grew at the interface were identified to be $(Cu,Ni)_6Sn_5$, Ni_2SnP, and Ni_3P. The inward diffusion of Sn to the Cu substrate followed by the formation of an additional IMC (Cu_6Sn_5) was induced by the Ni(P) depletion, thereby creating a multilayer IMC structure, $(Cu,Ni)_6Sn_5/Ni_2SnP/Ni_3P/Cu_6Sn_5$, at the interface. Additionally, the phase transformation of Ni_3P into Ni_2SnP also occurred with the in-diffusion of Sn, which resulted in the rapid growth of the Ni_2SnP phase and a gradual reduction in the Ni_3P phase. This mechanism Ni(P)-depletion-induced Ni_2SnP growth and Ni_3P reduction is unique among the reaction mechanisms established in the literature. We proposed a two-stage reaction mechanism based on the mass conservation of P, which provided a rationalization of this unique IMC growth behavior induced by Ni(P) depletion. The results of this study provide information on the microstructure evolution and phase transformation of a submicron Ni(P) film during soldering reaction, which might advance the understanding of the solderability of an ultrathin Ni(P) surface finish in micro-electronic packaging applications.

ACKNOWLEDGEMENTS

This work was supported by the Ministry of Science and Technology (R.O.C.) under Grant Nos. MOST103-2221-E-155-010 and NSC103-2622-E-155-001. The authors would also like to acknowledge Chia-Wei Fan (Yuan Ze University), Wei-Hsiang Wu (Yuan Ze University), Dr. Richard Tseng (Kinsus Interconnect Technology Co.), John Lin (Kinsus Interconnect Technology Co.), Chung-Yuan Kao (National Taiwan University), and S. Y. Tsai (National Tsing Hua University) for their assistances in the experiments.

REFERENCES

1. X. Chen, *IEEE Microw. Wirel. Compon. Lett.* **17**, 94 (2007).
2. X. Wu, D. Cullen, G. Brist, and O. Ramahi, *IEEE Trans. Adv. Packag*. **31**, 182 (2008).
3. H. W. Deng, Y. J. Zhao, C. J. Liang, W. S. Jiang, and Y. M. Ning, *Prog. Electromagn. Res. M* **9**, 1 (2009).
4. C. E. Ho, C. W. Fan, W. H. Wu, and T. T. Kuo, *Thin Solid Films* **529**, 364 (2013).
5. C. E. Ho, S. J. Wang, C. W. Fan, and W. H. Wu, *J. Electron. Mater.* **43**, 16 (2014).
6. C. E. Ho, C. W. Fan, and W. Z. Hsieh, *Surf. Coat. Technol.* **259**, 244 (2014).
7. C. Y. Ho, J. G. Duh, C. W. Lin, C. J. Lin, Y. H. Wu, H. C. Hong, and T. H. Wang, *J. Mater. Sci.* **48**, 2724 (2013).
8. C. Y. Ho and J. G. Duh, *Mater. Sci. Eng.,* A **611**, 162 (2014).

9. S. P. Peng, W. H. Wu, C. E. Ho, and Y. M. Huang, *J. Alloy Compd.* **493**, 431 (2010).
10. W. H. Wu, C. S. Lin, S. H. Huang, and C. E. Ho, *J. Electron. Mater.* **39**, 2387 (2010).
11. Y. M. Kim, J. Y. Park, and Y. H. Kim, *J. Electron. Mater.* **41**, 763 (2012).
12. C. E. Ho, Y. C. Lin, and S. J. Wang, *Thin Solid Films* **544**, 551 (2013).
13. C. E. Ho, T. T. Kuo, C. C. Wang, and W. H. Wu, *Electron. Mater. Lett.* **8**, 495 (2012).
14. C. E. Ho, C. C. Wang, M. A. Rahman, and Y. C. Lin, *Thin Solid Films* **529**, 369 (2013).
15. K. Nogita, C. M. Gourlay, and T. Nishimura, *JOM* **61**, 45 (2009).
16. J. W. Yoon and S. B. Jung, *J. Alloys Compd.* **396**, 122 (2005).
17. Y. C. Lin and J. G. Duh, *Scripta Mater.* **54**, 1661 (2006).
18. Y. C. Lin, T. Y. Shih, S. K. Tien, and J. G. Duh, *Scripta Mater.* **56**, 49 (2007).
19. Y. C. Lin, K. J. Wang, and J. G. Duh, *J. Electron. Mater.* **39**, 283 (2010).
20. Z. P. Xia, Y. Lin, and Z. Q. Li, *Mater. Charact.* **59**, 1324 (2008).
21. Y. Yang, J. N. Balaraju, S. C. Chong, H. Xu, C. Liu, V. V. Silberschmidt, and Z. Chen, *J. Alloys Compd.* **565**, 11 (2013).
22. Y. Yang, J. N. Balaraju, Y. Huang, H. Liu, and Z. Chen, *Acta Mater.* **71**, 69 (2014).
23. S. H. Huh, K. D. Kim, K. S. Kim, and J. S. Jang, *Electron. Mater. Lett.* **16**, 1161 (2012).
24. R. M. Allen and J. B. VanderSande, *Scripta Mater.* **16**, 1161 (1982).
25. K. C. Huang, F. S. Shieu, Y. H. Hsiao, and C. Y. Liu, *J. Electron. Mater.* **41**, 172 (2012).
26. A. Kumar, Z. Chen, S. G. Mhaisalkar, C. C. Wang, P. S. Teo, and V. Kripesh, *Thin Solid Films* **504**, 410 (2006).
27. C. E. Ho, W. H. Wu, C. C. Wang, and Y. C. Lin, *J. Electron. Mater.* **41**, 3266 (2012).